Application of Optimal Control to Time-Resolution Protocol for Quantum Sensing

Chungwei Lin^{1*}, Qi Ding², Yanting Ma¹
Mitsubishi Electric Research Laboratories (MERL), 201 Broadway, Cambridge, MA 02139 and

²Department of Electrical Engineering and Computer Science,
Massachusetts Institute of Technology, Cambridge, MA 02139, USA

(Dated: November 4, 2025)

Time-resolution protocol of quantum sensing aims to measure the fast temporal variation of an external field and demands a high field sensitivity in a short interrogation time τ . Since any operation that evolves the quantum state takes time and is counted as part of the interrogation, evaluating the performance of time-resolution protocol requires a complete end-to-end description of the measurement process. In particular, the initial state has to be one of the quantum sensor's eigenstates in the absence of external fields, and the final projective measurements must be performed in the same eigenstate basis. Building upon prior works which proposed limits for time-resolved sensing using a quantum sensor, we apply optimal control theory to optimize the time-resolution protocol. Our analysis indicates that there exists a critical interrogation time T^* : when $\tau < T^*$ the optimal protocol is purely bang-bang; when $\tau > T^*$ the optimal protocol involves a singular control during the interrogation. In the short- τ regime, which is relevant to high time resolution, we propose a "detune protocol" that involves only smooth control during the entire interrogation. As the discontinuities of control pose the main obstacles to experimental realization, we expect the presented detune protocol to be practically useful. In the long- τ regime, the optimal protocol closely resembles the Ramsey sequence; protocols based on maximizing Quantum Fisher Information are constructed to highlight the difference between the theoretically optimal and practically implementable measurements. Effective use of the time-resolution protocol requires a setup where the unknown time-domain signal of interest can be identically and repeatedly generated. As a potentially relevant application, we outline the calibration of baseband flux pulse distortion in the control of superconducting qubits.

I. INTRODUCTION

Quantum sensing generally refers to the technology that explicitly makes use of quantum phenomena to achieve highly sensitive and precise measurement [1]. Notable examples include employing the squeezed state of light to enhance the sensitivity of laser interferometers [2–6], using Nitrogen-Vacancy (NV) centers in diamond to measure signals generated by sub-micron objects [7–10], and utilizing the multi-level interference spectroscopy of Rydberg atoms to determine the amplitude of microwave and terahertz electromagnetic signals [11–18]. Intrinsic quantum advantage amounts to identifying and preparing the quantum state that is most sensitive to the field to be measured. The sensing performance can be quantified by the Quantum Fisher Information (QFI) [19, 20]; given an unbiased estimator, the inverse of QFI gives the lower bound (Cramér-Rao bound) of the variance of the parameter to be estimated. QFI, which depends solely on the quantum state and not on the specific measurement observables, is very valuable in both formal analysis and numerical simulations. From a theoretical point of view, QFI provides a framework for comparing performances of different states. Given a sensing setup, analysis of QFI identifies its theoretical bound (known as the Heisenberg limit) and the corresponding best-sensing state (equal superposition of eigenstates with the largest and smallest eigenvalues) [21, 22]. From a practical perspective, maximizing QFI over the available control parameters offers a concrete means – or at least a guide – for approaching the quantum limit [23–27].

For realistic implementations, both the initial state and the measurement observable have to be specified to determine the overall sensing performance; they are especially essential for the time-resolution protocols. The objective of the time-resolution protocol is to maximize the sensitivity with respect to the to-be-measured field in a short interrogation time τ . Because any operation that evolves the quantum state takes time, the description of the time-resolution protocol should begin with the quantum sensor in one of its eigenstates in the absence of external fields, and end up with a projective measurement in the same eigenstate basis. In Ref. [28], Herb and Degen propose a time-resolution protocol based on the Ramsey sequence [29] and the Rotating Wave Approximation (RWA). Their protocol, which

^{*} clin@merl.com

will be served as the reference for comparison, consists of two sequential pulses of equal duration, one corresponding to $\hat{\sigma}_y$ and the other to $\hat{\sigma}_x$ in the rotating frame, and has been experimentally demonstrated [30].

In this work, we apply Optimal Control Theory (OCT) to analyze the time-resolution protocol. OCT provides an efficient way to minimize a user-defined terminal cost subject to the dynamics that contains a time-dependent scalar control [31-34]. It has emerged as a valuable tool for engineering a wide range of quantum systems [35-38], such as stabilizing ultracold molecules [39], optimizing the performance in nuclear magnetic resonance measurement [40–42], cooling of quantum systems [43–45], and enhancing the yield of the target product in a chemical process [46–49]. Apart from the better sensitivity, which is expected as the optimal control gives the best possible performance, the general behavior of the optimal protocols is qualitatively similar to that of the reference protocols. In the short- τ regime which is relevant to high time resolution, we propose a detune protocol that only involves the smooth control field over the entire interrogation and performs comparably to the reference protocol. Given that discontinuities in the control field pose the primary experimental challenge, we expect the detune protocol to be practically useful. One bottleneck of meaningfully utilizing the time-resolution protocol is the need to generate the *identical*, yet unknown time-domain signal repeatably. We suggest that it can be used to calibrate the pulse distortion in fast flux control in superconducting qubits [50–52], which is an essential but cumbersome process for calibrating quantum gates, and is increasingly detrimental as the number of qubits gets larger. We discuss the potential to substantially reduce the total calibration time by leveraging our protocol to perform sequential measurements of the same distorted pulse. The rest of the paper is organized as follows. Section II defines the problem of time resolution and provides the necessary background. Section III presents our main results, including the general behavior from optimal control and a detailed description of the detune protocol. Section IV discusses practical aspects, including an outline of a realistic application. Section V provides a brief conclusion.

II. PROBLEM STATEMENT AND OPTIMAL CONTROL

A. Overview and problem statement

In this subsection we formulate the design of the time-resolution protocol for quantum sensing as an optimal control problem. The quantum sensor is modeled as a two-level system, which can physically correspond to an electron spin, an atom, or a superconducting qubit; it is described by the Hamiltonian [28]

$$H = \frac{\omega_0 + \delta\omega}{2}\hat{\sigma}_z + u(t)\hat{\sigma}_x. \tag{1}$$

where ω_0 is the natural angular frequency of the quantum sensor, $\delta\omega$ is the field which we want to measure, and u(t) is a scalar field which we can control. We shall take $\hbar\equiv 1$, $\omega_0\equiv 1$ in our simulations but explicitly keep ω_0 in all expressions; within this convention energy is measured in units of $\hbar\omega_0$ and time ω_0^{-1} . $|0\rangle$ and $|1\rangle$ are eigenstates of $\hat{\sigma}_z$ with eigenvalues of 1 and -1 respectively. They are eigenstates without external fields (i.e., $\delta\omega=u=0$) and will be referred to as the natural eigenstates of the quantum sensor.

The performance of the time-resolution protocol is quantified by its measurement sensitivity with respect to $\delta\omega$ given an (short) interrogation time τ . Because any operation contributes to the interrogation time, an end-to-end description of the measurement process is required for performance evaluation. In particular the initial state and the basis of the final projection measurement have to be the sensor's natural eigenstates. Without loss of generality we choose the initial state to be $|0\rangle$ and measure the probability that ends up with the same $|0\rangle$ state; the outcome probability can be expressed as

$$p(\delta\omega) \equiv |\langle 0|U[u;\delta\omega]|0\rangle|^{2}$$

$$\approx \underbrace{|\langle 0|U[u]|0\rangle|^{2}}_{\equiv p_{0}} + \underbrace{(\delta\omega)\frac{\partial}{\partial(\delta\omega)}|\langle 0|U[u]|0\rangle|^{2}}_{\equiv \delta p}$$

$$\approx p_{0} + \eta \cdot (\delta\omega). \tag{2}$$

 p_0 is the probability with zero field (i.e., $\delta\omega=0$) and is independent of $\delta\omega$; the linear coefficient of $\delta\omega$, denoted as η ,

is the "measurement sensitivity" [28]:

$$\eta = \frac{\partial}{\partial(\delta\omega)} |\langle 0|U[u]|0\rangle|^2. \tag{3}$$

Larger $|\eta|$ implies a greater capability of detecting a small signal. For the rest of paper we take $\eta = |\eta|$ and neglect its sign. When $\delta\omega$ is small, the linear approximation is sufficient and the unbiased estimator of $\delta\omega$ is given by

$$\delta\omega = \frac{p - p_0}{\eta}.\tag{4}$$

In terms of optimization, the objective is to find the protocol u(t) that maximizes the amplitude of sensitivity $|\eta|$ or η^2 , given an interrogation time τ and an amplitude constraint u_{max} . We will apply OCT to obtain the optimal protocol and its corresponding maximum sensitivity. Having identified the best possible performance, we introduce a smooth but sub-optimal "detune protocol" that addresses experimental feasibility. It is worth pointing out that the ultimate goal of time-resolution protocol is to reconstruct an unknown $\delta\omega(t)$ via $p(\delta\omega(t))$, but to measure $p(\delta\omega(t))$ requires repeatedly generating an identical yet unknown $\delta\omega(t)$. Identifying realistic settings that satisfy these conditions is also part of the problem, and we shall consider a potentially meaningful application in Section IV B.

B. Reference: resonant YX protocol

The reference protocol, which will be termed as the resonant YX protocol or simply the YX protocol, is the one proposed by Herb and Degen in Ref. [28]; its control waveform is

$$u_{\rm YX}(t) = \begin{cases} u_{\rm max} \cos(\omega_0 t + \frac{\pi}{2}) & 0 \le t \le \min(\frac{\tau}{2}, \frac{t_{\rm QSL}}{2}) \\ 0 & \min(\frac{\tau}{2}, \frac{t_{\rm QSL}}{2}) \le t \le \max(\frac{\tau}{2}, \tau - \frac{t_{\rm QSL}}{2}) \\ u_{\rm max} \cos(\omega_0 t) & \max(\frac{\tau}{2}, \tau - \frac{t_{\rm QSL}}{2}) \le t \le \tau \end{cases}$$
 (5)

where $t_{\text{QSL}} = \frac{\pi}{u_{\text{max}}}$ is referred to as the quantum speed limit [28, 53–56]. The rationale behind the protocol naming is as follows: the "resonant" indicates that the applied frequency is identical to the natural frequency; "YX" that in RWA, $\cos(\omega_0 t + \frac{\pi}{2})\hat{\sigma}_x$ and $\cos(\omega_0 t)\hat{\sigma}_x$ respectively lead to $\hat{\sigma}_y$ (Y operation) and $\hat{\sigma}_x$ (X operation) in the rotating frame. Overall the YX protocol identifies a critical interrogation time t_{QSL} , below which the protocol is composed of equal-duration Y and X operations, and above which the protocol involves a free evolution between Y and X operations.

With RWA, the sensitivity of the YX protocol grants an analytical expression

$$\eta_{\text{YX,RWA}}(\tau) = \begin{cases} \frac{t_{\text{QSL}}}{\pi} \sin(\frac{\pi}{2} \frac{\tau}{t_{\text{QSL}}}) \left(1 - \cos(\frac{\pi}{2} \frac{\tau}{t_{\text{QSL}}})\right) & \tau < t_{\text{QSL}} \\ \frac{t_{\text{QSL}}}{2} \left(\frac{\tau}{t_{\text{QSL}}} - \left(1 - \frac{2}{\pi}\right)\right) & \tau > t_{\text{QSL}} \end{cases}$$
(6)

Since η has the dimension of time, it is suitable to introduce a dimensionless measure $\frac{\eta}{\tau}$. When expressed in the dimensionless time variable $\tilde{\tau} \equiv \frac{\tau}{t_{\rm OSL}}, \frac{\eta}{\tau}$ is given by

$$\frac{\eta_{\text{YX,RWA}}}{\tau} = \begin{cases} \frac{\tilde{\tau}^{-1}}{\pi} \sin(\frac{\pi}{2}\tilde{\tau}) \left(1 - \cos(\frac{\pi}{2}\tilde{\tau})\right) & \tilde{\tau} < 1\\ \frac{\tilde{\tau}^{-1}}{2} \left(\tilde{\tau} - \left(1 - \frac{2}{\pi}\right)\right) & \tilde{\tau} > 1 \end{cases}$$
 (7)

Eq. (7) has no explicit u_{max} dependence and approaches $\frac{1}{2}$ as $\tilde{\tau} \to \infty$. When comparing performances of different u_{max} 's, τ 's, and protocols, it is convenient to plot $\frac{\eta}{\tau}$ as a function of $\frac{\tau}{t_{\text{QSL}}}$; this convention will be adopted in this work and Eq. (7) will be served as the baseline.

When designing the protocol we assume that $\delta\omega$ stays unchanged during the entire (short) interrogation τ , thus within this setting τ is the minimum time that a time-resolution protocol can resolve. Once the protocol is fixed, however, a more general expression that includes the fast time variation of $\delta\omega$ is given by

$$\delta p(\delta \omega) = \int_{t-\tau/2}^{t+\tau/2} dt' K(t'-t) \cdot \delta \omega(t'). \tag{8}$$

Here K is a protocol dependent convolution kernel; for constant $\delta\omega$ one recovers $\eta = \int_{-\tau/2}^{\tau/2} dt K(t)$. In Appendix A (see also Supplementary of Ref. [28]) we provide a simple numerical method to construct the kernel of Eq. (8). Once K is known, the time resolution shorter than τ is in principle possible [30].

To facilitate the subsequent discussion we explain our subscript naming convention. The sensitivity η can be evaluated using different protocols and approximations; they are indicated in the subscript by η Protocol, Approximation. In this work, 'Protocol' can be one of (i) YX (reference), (ii) D (detune), or (iii) Opt (optimal); 'Approximation' can be either (i) RWA or (ii) full calculation (no approximation). We neglect the second subscript for full calculation. For example, η_D is obtained using the detune protocol and full calculation.

C. Optimal control

In this subsection we summarize the important functions introduced in OCT. Numerous comprehensive reviews have been reported in the literature [36, 37], and its applications specific to the unitary qubit can be found in Ref. [57]. Here, special attention is devoted to the cost function that involves a derivative of the wave function.

The sensitivity η characterizes the sensing performance and is the most important quantity to evaluate. Its explicit dependence on the final-time wave function $|\psi_0(\tau)\rangle$ is given by

$$\eta = \frac{\partial}{\partial(\delta\omega)} \left[\langle 0|\psi_0(\tau)\rangle \langle \psi_0(\tau)|0\rangle \right]
= \langle 0|\psi_1(\tau)\rangle \langle \psi_0(\tau)|0\rangle + \langle 0|\psi_0(\tau)\rangle \langle \psi_1(\tau)|0\rangle,$$
where $|\psi_1(t)\rangle \equiv \frac{\partial}{\partial(\delta\omega)} |\psi_0(t)\rangle.$
(9)

Optimizing the time-resolution protocol is equivalent to maximizing $|\eta|$. To avoid dealing with sign of η we choose to maximize η^2 or equivalently to minimize the terminal cost function

$$\mathcal{C}_{\eta^2} = -\frac{1}{2}\eta^2 = -\frac{1}{2} \left\{ \frac{\partial}{\partial(\delta\omega)} \left[\langle 0|\psi_0(\tau)\rangle\langle\psi_0(\tau)|0\rangle \right] \right\}^2 \\
= -\frac{1}{2} \left(\langle 0|\psi_1(\tau)\rangle\langle\psi_0(\tau)|0\rangle + \langle 0|\psi_0(\tau)\rangle\langle\psi_1(\tau)|0\rangle \right)^2.$$
(10)

The optimization problem can now be formally specified:

Find $u^*(t)$ that minimizes $\mathcal{C}_{\eta^2}[u(t)]$ subject to

(i) dynamics
$$i\partial_t |\psi_0(t)\rangle = \left[\frac{\omega_0 + \delta\omega}{2}\hat{\sigma}_z + u(t)\hat{\sigma}_x\right]|\psi_0(t)\rangle,$$

(ii) initial state $|\psi(0)\rangle = |0\rangle,$ (11)

- (iii) total interrogation time τ ,
- (vi) amplitude constraint $|u(t)| \leq u_{\text{max}}$.

OCT is a powerful tool for dynamics-constrained optimization. Given the dynamics and the cost to minimize, it introduces the adjoint variables $|\pi(t)\rangle$, the control-Hamiltonian $\mathcal{H}_{\text{oc}}(t)$, and the switching function $\Phi(t)$ [defined shortly in Eqs. (12)] that are computationally accessible and accurately characterize the system response to some external or model variables. One non-trivial complication from the cost \mathcal{C}_{η^2} is its dependence on $|\psi_1(\tau)\rangle = \frac{\partial}{\partial(\delta\omega)}|\psi_0(\tau)\rangle$. To cope with this additional dependence we augment the system by regarding $|\psi_0\rangle$ and $|\psi_1\rangle$ as independent variables; more details can be found in Ref. [26, 58].

Denote the variables in augmented dynamics as $|\psi\rangle = \begin{bmatrix} |\psi_0\rangle \\ |\psi_1\rangle \end{bmatrix}$ and its adjoint variables as $|\pi\rangle = \begin{bmatrix} |\pi_0\rangle \\ |\pi_1\rangle \end{bmatrix}$, the OCT

for a general terminal cost $\mathcal{C}(|\psi_0(\tau)\rangle, |\psi_1(\tau)\rangle)$ is summarized as follows.

$$\mathcal{H}_{\rm oc}(t) = \operatorname{Im} \left\{ \begin{bmatrix} \langle \pi_0 | \langle \pi_1 | \end{bmatrix} \begin{bmatrix} H_0 & 0 \\ \frac{\hat{\sigma}_z}{2} & H_0 \end{bmatrix} \begin{bmatrix} |\psi_0 \rangle \\ |\psi_1 \rangle \end{bmatrix} \right\} \sim \frac{\partial \mathcal{C}}{\partial \tau}, \tag{12a}$$

$$\Phi(t) = \operatorname{Im} \left\{ \begin{bmatrix} \langle \pi_0 | \langle \pi_1 | \end{bmatrix} \begin{bmatrix} \hat{\sigma}_x & 0 \\ 0 & \hat{\sigma}_x \end{bmatrix} \begin{bmatrix} |\psi_0 \rangle \\ |\psi_1 \rangle \end{bmatrix} \right\} = \frac{1}{\operatorname{d}t} \frac{\delta \mathcal{C}}{\delta u(t)}, \tag{12b}$$

$$\partial_t \begin{bmatrix} |\psi_0\rangle \\ |\psi_1\rangle \end{bmatrix} = -i \begin{bmatrix} H_0 & 0 \\ \frac{\hat{\sigma}_z}{2} & H_0 \end{bmatrix} \begin{bmatrix} |\psi_0\rangle \\ |\psi_1\rangle \end{bmatrix} \text{ with } \begin{bmatrix} |\psi_0(0)\rangle \\ |\psi_1(0)\rangle \end{bmatrix} = \begin{bmatrix} |0\rangle \\ 0 \end{bmatrix}, \tag{12c}$$

$$\partial_t \begin{bmatrix} |\pi_0\rangle \\ |\pi_1\rangle \end{bmatrix} = -i \begin{bmatrix} H_0 & \frac{\hat{\sigma}_z}{2} \\ 0 & H_0 \end{bmatrix} \begin{bmatrix} |\pi_0\rangle \\ |\pi_1\rangle \end{bmatrix} \text{ with } \begin{bmatrix} |\pi_0(\tau)\rangle \\ |\pi_1(\tau)\rangle \end{bmatrix} = 2 \begin{bmatrix} \frac{\partial \mathcal{C}}{\partial (\psi_0(\tau))} \\ \frac{\partial \mathcal{C}}{\partial (\psi_1(\tau))} \end{bmatrix}, \tag{12d}$$

where $H_0 = H(\delta\omega = 0) = \frac{\omega_0}{2}\hat{\sigma}_z + u(t)\hat{\sigma}_x$. Terminal cost determines the final-time condition of the adjoint variables $|\pi\rangle$. Two terminal costs will be considered. To maximize the sensitivity we choose $\mathcal{C} = \mathcal{C}_{\eta^2}$ so that

$$\begin{bmatrix}
|\pi_0(\tau)\rangle \\
|\pi_1(\tau)\rangle
\end{bmatrix} = 2 \begin{bmatrix}
\frac{\partial \mathcal{C}_{\eta^2}}{\partial \langle \psi_0(\tau)|} \\
\frac{\partial \mathcal{C}_{\eta^2}}{\partial \langle \psi_1(\tau)|}
\end{bmatrix} = -4 \operatorname{Re} \left[\langle 0|\psi_0(T)\rangle \langle \psi_1(T)|0\rangle \right] \begin{bmatrix}
|0\rangle \langle 0|\psi_1(\tau)\rangle \\
|0\rangle \langle 0|\psi_0(\tau)\rangle
\end{bmatrix}.$$
(13)

We also consider maximizing QFI [26] where the terminal cost is negative QFI:

$$\mathcal{C}_{\text{QFI}} = -\text{QFI} = -4 \left[\langle \psi_{1}(\tau) | \psi_{1}(\tau) \rangle - | \langle \psi_{0}(\tau) | \psi_{1}(\tau) \rangle|^{2} \right],
\begin{bmatrix} |\pi_{0}(\tau)\rangle \\ |\pi_{1}(\tau)\rangle \end{bmatrix} = 2 \begin{bmatrix} \frac{\partial \mathcal{C}_{\text{QFI}}}{\partial \langle \psi_{0}(\tau) | \rangle} \\ \frac{\partial \mathcal{C}_{\text{QFI}}}{\partial \langle \psi_{1}(\tau) | \rangle} \end{bmatrix} = 8 \begin{bmatrix} |\psi_{1}(\tau)\rangle \langle \psi_{1}(\tau) | \psi_{0}(\tau)\rangle, \\ -|\psi_{1}(\tau)\rangle + |\psi_{0}(\tau)\rangle \langle \psi_{0}(\tau) | \psi_{1}(\tau)\rangle \end{bmatrix}.$$
(14)

In Section IIID we present the results from protocols that maximizes QFI.

Eqs. (12) plus Eq. (13) [or Eq. (14)] completely determine quantities introduced by OCT. They are used to express two general optimality conditions [59]. First, the optimal control is

$$u^*(t) = \begin{cases} -u_{\text{max}} \operatorname{Sgn}[\Phi] & \text{if } \Phi \neq 0, \text{ bang (B) control} \\ u^{\sin}(t) & \text{if } \Phi = 0, \text{ singular (S) control} \end{cases}, \tag{15}$$

where Sgn denotes the sign function. The values of singular control u^{sing} need to be determined numerically, but OCT provides the following expression [see Appendix B for the derivation]

$$u^{\text{sing}}(t) = \frac{\omega_0}{2} \frac{\text{Im}[\langle \pi | \begin{bmatrix} 0 & 0 \\ \hat{\sigma}_x & 0 \end{bmatrix} | \psi \rangle]}{\text{Im}[\langle \pi | \begin{bmatrix} \frac{\omega_0}{2} \hat{\sigma}_z & 0 \\ \frac{1}{2} \hat{\sigma}_z & \frac{\omega_0}{2} \hat{\sigma}_z \end{bmatrix} | \psi \rangle]},\tag{16}$$

which is very valuable for numerics. Second, for an optimal solution, $\mathcal{H}_{oc}(t)$ is a constant over the entire evolution and its value is proportional to the derivative of the terminal cost function with respect to the interrogation time τ . For both \mathcal{C}_{η^2} and \mathcal{C}_{QFI} , the resulting \mathcal{H}_{oc} 's are always negative as increasing τ always increases $\eta^2(\tau)$ and $QFI(\tau)$.

We emphasize that although the physical system considered here is equivalent to a qubit with unitary dynamics [i.e., Eq. (1)], the augmented dynamics specified in Eq. (12c) is neither planar (i.e., two real-valued variables) nor unitary. For these reasons certain properties specific to the unitary qubit given in Ref. [57] do not hold anymore. Particularly we point out that the BB control does *not* have identical bang duration and the singular control does *not* require $u^{\text{sing}} = 0$.

D. Practical use of OCT functions

We conclude this section by highlighting the usefulness of OCT. The most practically useful quantity is undoubtedly the switching function Φ . By sequentially solving the dynamics twice, one forward in time for $|\psi\rangle$ and one backward $|\pi\rangle$, one is able to obtain the gradient of \mathcal{C} with respect to all $u(t_i)$ [60]. Three applications used in the work are

highlighted. First Φ is primarily used to construct a numerical $u^*(t)$ by some gradient-based (or quasi-Newton) algorithm that involves

$$u^{(n+1)}(t) \to u^{(n)}(t) - \text{updating rate} \times \Phi.$$
 (17)

For the free-form parametrization one divides τ into N_t intervals and assumes a piecewise constant waveform. In our simulations N_t ranges from 100 to 2000 (depending on τ); we ensure that the result has a negligible change upon increasing N_t 's and that N_t is sufficiently large so that all optimality conditions are numerically satisfied [26]. Empirically we find that when $u^*(t)$ contains both B and S controls, the convergence of S control is slow due to its vanishing gradient. In this case we can compute Eq. (16) at nth iteration, and replace the non-bang controls by the singular values:

$$u^{(n+1)}(t) \to u^{\sin(n)}(t) \text{ for } |u^{(n)}(t)| < u_{\text{max}}.$$
 (18)

Including Eq. (18) greatly accelerates the convergence.

Second, quite often the feasible control waveform is constrained by the hardware and is conveniently parametrized by $u(t; \vec{\alpha})$; the objective in this case reduces to optimizing the performance within the parametrized control space. The gradient $\frac{\partial \mathcal{C}}{\partial \vec{\sigma}}$ can be computed by

$$\frac{\partial \mathcal{C}}{\partial \vec{\alpha}} = \sum_{t} \frac{\partial \mathcal{C}}{\partial u(t)} \frac{\partial u(t; \vec{\alpha})}{\partial \vec{\alpha}} = \sum_{t} dt \, \Phi(t) \frac{\partial u(t; \vec{\alpha})}{\partial \vec{\alpha}} = \int_{0}^{\tau} dt \, \Phi(t) \frac{\partial u(t; \vec{\alpha})}{\partial \vec{\alpha}}. \tag{19}$$

One then uses some gradient-based algorithm to find the solution. Eq. (19) will be used to construct the best detune protocol [see Section III C].

Third, Φ can be used to estimate the deviation in performance caused by the imperfect control. For this application, one computes $\Phi_{\text{ref}}(t)$ using the reference control $u_{\text{ref}}(t)$. If the applied control $u_{\text{app}}(t)$ is different from the reference control, the resulting change in cost can be estimated by

$$C[u(t)] - C[u_{\text{ref}}(t)] = \sum_{i} \frac{\partial C}{\partial u_{i}} [u_{\text{app}}(t_{i}) - u_{\text{ref}}(t_{i})] = \int_{0}^{\tau} dt \, \Phi_{\text{ref}}(t) [u_{\text{app}}(t) - u_{\text{ref}}(t)]. \tag{20}$$

Eq. (20) can be used to estimate the performance reduction due to non-ideal switching times in BB protocol. It will be used to estimate the effect of smoothness (or uncertainty of exact switching times in BB protocols) in Section IV A.

Two practical utilizations of control-Hamiltonian $\mathcal{H}_{oc}(t) \sim \frac{\partial \mathcal{C}}{\partial \tau}$ are outlined. First, the deviation from a constant $\mathcal{H}_{oc}(t)$ can be used to quantify the solution quality [26]. Second, in a damped quantum system $\mathcal{H}_{oc} = 0$ offers a rigorous criterion for defining the optimal operation time for a quantum task [27].

III. OPTIMAL PROTOCOL AND REALISTIC PROTOCOL

A. Overview and general behavior

This section contains our main results which include the performance of the optimal protocol and the detune protocol: the former represents the best sensitivity the system can possibly achieve; the latter is a *smooth* protocol with performance comparable to that of the reference YX protocol.

The overall behavior of optimal protocols is illustrated in Fig. 1(a) where the optimal $\frac{\eta}{\tau}$ for $u_{\rm max}$ =0.1, 0.2, 0.5 and the reference YX protocol [using RWA, see Eq. (7)] are plotted. It is seen that the metrological gain of optimal control is more significant for the short interrogation time. Similar to the YX protocol, the optimal protocol introduces a critical interrogation time T^* . When $\tau < T^*$ the optimal protocol is exclusively BB; when $\tau > T^*$ the optimal protocol involves a singular control in the middle, resembling the free evolution in the Ramsey protocol. Two representative control waveforms are illustrated in Fig. 1(b) and (c) where the optimal protocols for $\tau = 0.6\,t_{\rm QSL}$ and $1.2\,t_{\rm QSL}$ are plotted. The optimality conditions are numerically verified in both cases. For the rest of this section, we provide more detailed analysis for both short ($\tau < T^*$) and long ($\tau > T^*$) interrogation times.

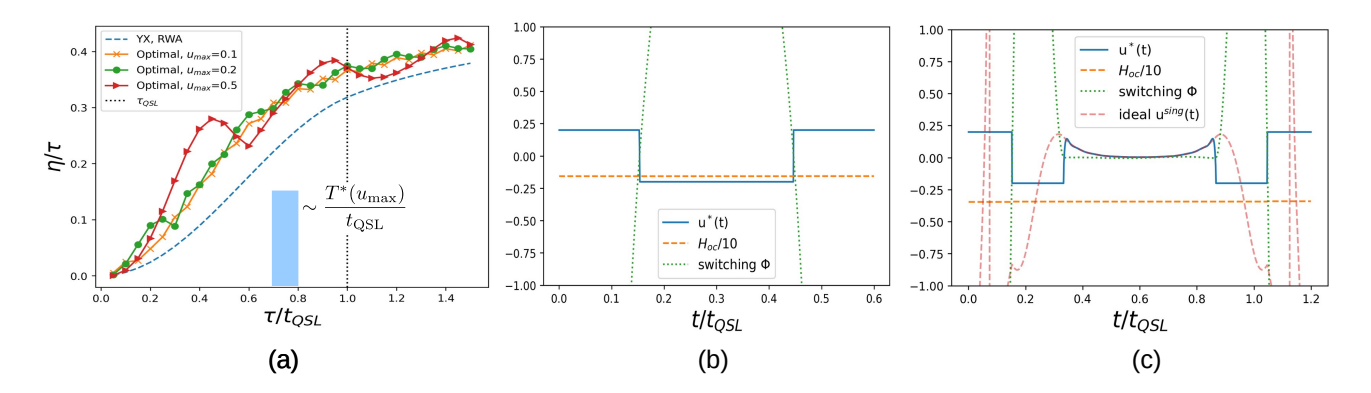


FIG. 1: $\eta_{\rm opt}/\tau$ for $u_{\rm max}=0.1,\,0.2,\,0.5$. The reference YX protocol using RWA is provided as the reference. The metrological gain of optimal protocol is more significant for short interrogation time, which is the regime relevant to high time resolution. The critical interrogation time T^* depends on $u_{\rm max}$ and is about 0.8 $t_{\rm QSL}$ ($t_{\rm QSL}=\frac{\pi}{u_{\rm max}}$) for $u_{\rm max}<0.2$ (blue area). (b) For $u_{\rm max}=0.2,\,\tau=0.6\,t_{\rm QSL}$, the optimal control is of BB. Optimality conditions are verified. (c) For $u_{\rm max}=0.2,\,\tau=1.2\,t_{\rm QSL}$, the optimal control includes a singular portion in the middle. Optimality conditions – Eq. (15) for B control, Eq. (16) for S control, and a constant $\mathcal{H}_{\rm oc}(t)$ – are numerically verified.

B. Short interrogation time $\tau < T^*$ I: detune protocol in RWA

One practical challenge in implementing the reference YX protocol is its discontinuity at the midpoint of the interrogation. In this subsection we present a *smooth* detune protocol and show that within RWA it can achieve performance comparable to that of the YX protocol. The detune protocol is given by

$$u_{\text{D,RWA}}(t) = u_{\text{max}}\cos(\omega t + \theta), \ 0 \le t \le \tau.$$
 (21)

The "detune" refers to the fact that the driving frequency $\omega/(2\pi)$ is different from the natural frequency $\omega_0/(2\pi)$; its value will be determined by maximizing the sensitivity η .

Applying the transformation $|\tilde{\psi}_0\rangle = e^{-i\frac{\hat{\sigma}_z}{2}\omega t}|\psi_0\rangle$ and neglecting the high-frequency terms, the resulting Schrödinger equation in the rotating frame is $i\partial_t|\tilde{\psi}_0\rangle = H_{\rm RWA}|\tilde{\psi}_0\rangle$ where the time-independent $H_{\rm RWA}$ is

$$H_{\text{RWA}} = \frac{\delta\omega - \Delta\omega}{2}\hat{\sigma}_z + \frac{u_{\text{max}}}{2} \left(\hat{\sigma}_x \cos\theta + \hat{\sigma}_y \sin\theta\right)$$

$$\equiv \frac{\tilde{\Omega}}{2} \left[\frac{\Delta}{\tilde{\Omega}}\hat{\sigma}_z + \frac{u_{\text{max}}}{\tilde{\Omega}} \left(\hat{\sigma}_x \cos\theta + \hat{\sigma}_y \sin\theta\right)\right]. \tag{22}$$

In Eq. (22) $\Delta \equiv \delta\omega - \Delta\omega = \delta\omega - (\omega - \omega_0)$ and $\tilde{\Omega}^2 = u_{\rm max}^2 + \Delta^2$; $\Delta\omega = \omega - \omega_0$ is the detune of the applied angular frequency. The evolution in the rotating frame and its first diagonal component are

$$e^{-iH_{\text{RWA}}\tau} = \cos(\frac{\tilde{\Omega}\tau}{2})\,\hat{e}_{2\times 2} - i\sin(\frac{\tilde{\Omega}\tau}{2}) \left[\frac{\Delta}{\tilde{\Omega}}\hat{\sigma}_z + \frac{u_{\text{max}}}{\tilde{\Omega}} \left(\hat{\sigma}_x \cos\theta + \hat{\sigma}_y \sin\theta \right) \right]$$

$$\Rightarrow \left| \langle 0|e^{-iH_{\text{RWA}}\tau}|0\rangle \right|^2 = \cos^2(\frac{\tilde{\Omega}\tau}{2}) + \sin^2(\frac{\tilde{\Omega}\tau}{2}) \cdot \frac{\Delta^2}{u_{\text{max}}^2 + \Delta^2}.$$
(23)

Eq. (23) shows that the phase θ is irrelevant as neither $\hat{\sigma}_x$ nor $\hat{\sigma}_y$ has diagonal components; this is not the case when using full calculation (next subsection). It is worth noting that $\left|\langle 0|e^{-iH_{\text{RWA}}\tau}|0\rangle\right|^2 = \left|\langle 1|e^{-iH_{\text{RWA}}\tau}|1\rangle\right|^2$, indicating the same protocol can apply to either natural eigenstate.

The sensitivity of the detune protocol in RWA, denoted as $\eta_{\text{D,RWA}}$, is given by

$$\eta_{\text{D,RWA}}(\Delta\omega) = \left[\frac{\partial}{\partial(\delta\omega)} \left| \langle 0|e^{-iH_{\text{RWA}}\tau}|0\rangle \right|^2 \right]_{\delta\omega=0}
= (\Delta\omega) \frac{u_{\text{max}}^2}{\bar{\Omega}^4} \times \left[\frac{\bar{\Omega}\tau}{2} \sin(\bar{\Omega}\tau) + \cos(\bar{\Omega}\tau) - 1 \right],$$
(24)

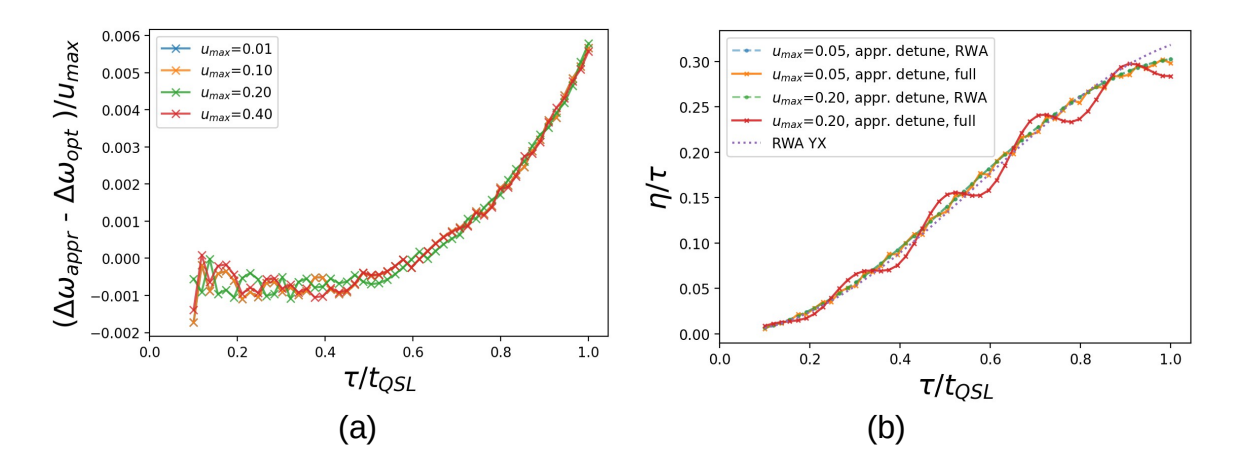


FIG. 2: Detune protocol within RWA. (a) The difference of detune values between directly optimizing Eq. (24) and the approximation of (26). (b) The resulting η/τ for $u_{\rm max}=0.05$ and 0.2. The difference between YX and detune protocols (RWA) is very small. The difference between detune protocols using RWA and the full calculation increases [using the approximate detune of (26)] as $u_{\rm max}$ increases.

with $\bar{\Omega}^2 = u_{\rm max}^2 + (\Delta\omega)^2$. $\eta_{\rm D,RWA}$ being an odd function in $\Delta\omega$ indicates that a minimum at $\eta_{\rm D,RWA}(\Delta\omega)$ guarantees a maximum at $\eta_{\rm D,RWA}(-\Delta\omega)$ with the same amplitude $|\eta_{\rm D,RWA}(\Delta\omega)| = |\eta_{\rm D,RWA}(-\Delta\omega)|$. One bears in mind that the RWA more accurately describes the blue-detuned regime $(\Delta\omega>0)$ as the neglect of high-frequency components is better justified. Introducing the dimensionless parameter $x\equiv\bar{\Omega}\tau=\sqrt{(u_{\rm max}\tau)^2+(\Delta\omega\cdot\tau)^2}\geq u_{\rm max}\tau$, Eq. (24) becomes

$$\frac{\left|\eta_{\text{D,RWA}}(x)\right|}{\tau} = (u_{\text{max}}\tau)^2 \sqrt{x^2 - (u_{\text{max}}\tau)^2} F(x) \text{ where}
F(x) = \frac{1}{x^4} \left[1 - \frac{x}{2} \sin(x) - \cos(x) \right].$$
(25)

F(x) is smooth at $x=0^+$ and positive for $0 < x < 2\pi$. The largest interrogation time we consider is $t_{\rm QSL}$. The optimal detune protocol within RWA is to find x and thus $\Delta\omega$ that maximizes $|\eta_{\rm D,RWA}|$; the optimized detune value depends on both $u_{\rm max}$ and τ . This can be done numerically and in the following we provide an analytical but accurate expression.

As a first-order approximation we assume the argmax $\eta_{\text{D,RWA}}(x) \gg u_{\text{max}}\tau$ so that $\sqrt{x^2 - (u_{\text{max}}\tau)^2} \approx x$. We can approximately maximize $\eta_0(x) = xF(x)$ and find $\underset{x}{\text{argmax}} \eta_0(x) = D_0 = 2.606$. With the same order of approximation, $D_0 = \Delta\omega\tau$ and thus $\Delta\omega \approx \frac{D_0}{\tau}$. This expression turns out to be good over for the entire $0 < \frac{\tau}{t_{\text{QSL}}} \le 1$. We numerically identify a small correction to this expression and the approximate detune is found to be

$$\Delta\omega_{\rm appr}(u_{\rm max}, \tau) \approx \frac{D_0}{\tau} - 0.02 \cdot u_{\rm max}^2 \tau$$
 (26)

The weak dependence on the $u_{\rm max}$ reflects the nature of RWA. The validity of Eq. (26) is examined by comparing $\Delta\omega_{\rm appr}$ with the optimal detune $\Delta\omega_{\rm opt}$ obtained by directly maximizing Eq. (24). Fig. 2(a) shows the difference between $\Delta\omega_{\rm appr}$ and $\Delta\omega_{\rm opt}$ is indeed small; Fig. 2(b) shows the resulting sensitivities are very close to those of YX protocols. To quantify the error caused by RWA we also compute the detune protocol using the full calculation. The discrepancy between RWA and full calculation becomes more significant upon increasing $u_{\rm max}$; for $\frac{u_{\rm max}}{\omega_0} < 0.2$, their difference is smaller than 15% when $\tau > 0.5\,t_{\rm QSL}$.

To provide some intuition, in Fig. 3 we visualize how the detune protocol enhances sensitivity by comparing trajectories of two detune protocols on the Bloch sphere where the sensor state in rotating frame is parametrized by $|\tilde{\psi}_0\rangle = \left[\cos\frac{\theta}{2},\sin\frac{\theta}{2}e^{i\phi}\right]^T$. Within RWA, the detune protocol has a time-independent Hamiltonian and each trajectory is associated with a rotating axis of the Bloch sphere. Using Eq. (22), given a detune $\Delta\omega$ and a to-be-measured field $\delta\omega$, the rotating axis is pointing along $(0,u_{\rm max},\delta\omega-\Delta\omega)$. The square of projection $\cos^2(\frac{\theta}{2})$ at the terminal point of the trajectory is the measurement signal. As a concrete example we consider $u_{\rm max}=0.2$ and $\tau=\frac{t_{\rm QSL}}{2}$. For the

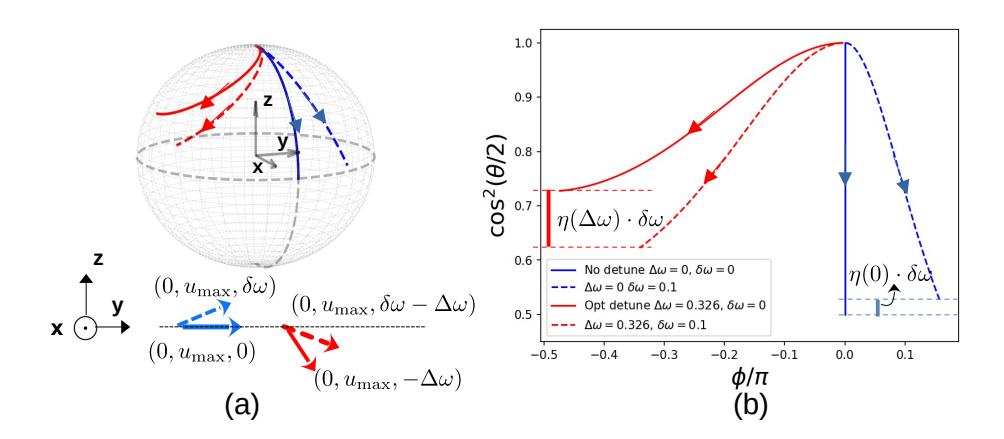


FIG. 3: Detune protocol in RWA and rotating frame. Trajectories on the Bloch sphere (a) and in ϕ -cos²($\theta/2$) plane (b). In both (a) and (b), the solid blue trajectory corresponds to the no-detune $\Delta\omega=0$ and zero-field $\delta\omega=0$ case; dashed blue to no-detune $\Delta\omega=0$ and finite-field $\delta\omega=0.1$; solid red to optimal-detune $\Delta\omega=0.326$ and zero-field $\delta\omega=0$; dashed red optimal-detune $\Delta\omega=0.326$ and finite-field $\delta\omega=0.1$. Within RWA, the detune protocol has a time-independent Hamiltonian and each trajectory corresponds to a rotating axis of the Bloch sphere. Bottom of (a) gives the rotating axes of four trajectories. The $\cos^2(\theta/2)$ is the measurement signal, and the difference at the end of interrogation with and without field quantifies the sensing performance. (b) In ϕ -cos²($\theta/2$) plane, the optimal detune (red) leads to a larger difference compared to the case of no detune (blue). The trajectories are computed using $u_{\text{max}}=0.2$, $\tau=0.5\,t_{\text{QSL}}=2.5\pi$.

zero detune $\Delta\omega=0$, the terminal points of two trajectories with $\delta\omega=0$ and 0.1 [blue curves in Fig. 3(a)] are both very close to the equator of Bloch sphere. Their projections on $|0\rangle$ are close [blue curves of Fig. 3(b)], indicating a low sensitivity for the field strength of $\delta\omega=0.1$. When using the optimal detune where $\Delta\omega\sim0.326$, the terminal point of $\delta\omega=0.1$ trajectory is close to equator [dash red curve in Fig. 3(a)] but that of $\delta\omega=0$ trajectory is not [solid red curve in Fig. 3(a)]. Their projections on $|0\rangle$ are more distinct [red curves of Fig. 3(b)], indicating an enhanced sensitivity for the field strength of $\delta\omega=0.1$.

C. Short interrogation time $\tau < T^*$ II: full calculation

We now use full calculation to obtain the best detune and optimal protocols in the $\tau < t_{\rm QSL}$ regime. With the full calculation, we re-parametrize the detune protocol [completely equivalent to Eq. (21)] as

$$u_{\rm D}(t;\omega,a) = u_{\rm max} \sin\left(\omega(t-\frac{\tau}{2}) + a\pi\right)$$

$$\Rightarrow \begin{cases} \frac{\partial u(t)}{\partial \omega} = -u_{\rm max} \sin\left(\omega(t-\frac{\tau}{2}) + a\pi\right) \cdot (t-\frac{\tau}{2}) \\ \frac{\partial u(t)}{\partial a} = -u_{\rm max} \sin\left(\omega(t-\frac{\tau}{2}) + a\pi\right) \cdot \pi \end{cases}$$
(27)

The applied frequency ω and a phase shift $a\pi$ are two tuning parameters. The gradients $\frac{\partial \mathcal{C}_{\eta^2}}{\partial \omega}$, $\frac{\partial \mathcal{C}_{\eta^2}}{\partial a}$ are computed using Eq. (19) and the second line of Eq. (27). The optimized (ω, a) for $u_{\text{max}} = 0.1$, 0.2 are shown in Fig. 4(b), (e). We stress again that the detune protocol has the identical performance for blue and red detunes in RWA; this is not true anymore in full calculation. Fig. 4(a), (d) show the sensitivity in $\frac{\eta}{\tau}$ obtained from the optimal, YX, and detune protocols using the full calculation. Certainly the optimal protocol has the largest $|\eta|$; the optimized detune protocol performs slightly better than the reference YX protocol. In terms of control waveform, the optimal protocol is BB which has a few discontinuities; the YX protocol has one discontinuity at the midpoint $t = \frac{\tau}{2}$; the detune protocol is smooth during the entire interrogation [see Fig. 4(c), (f)].

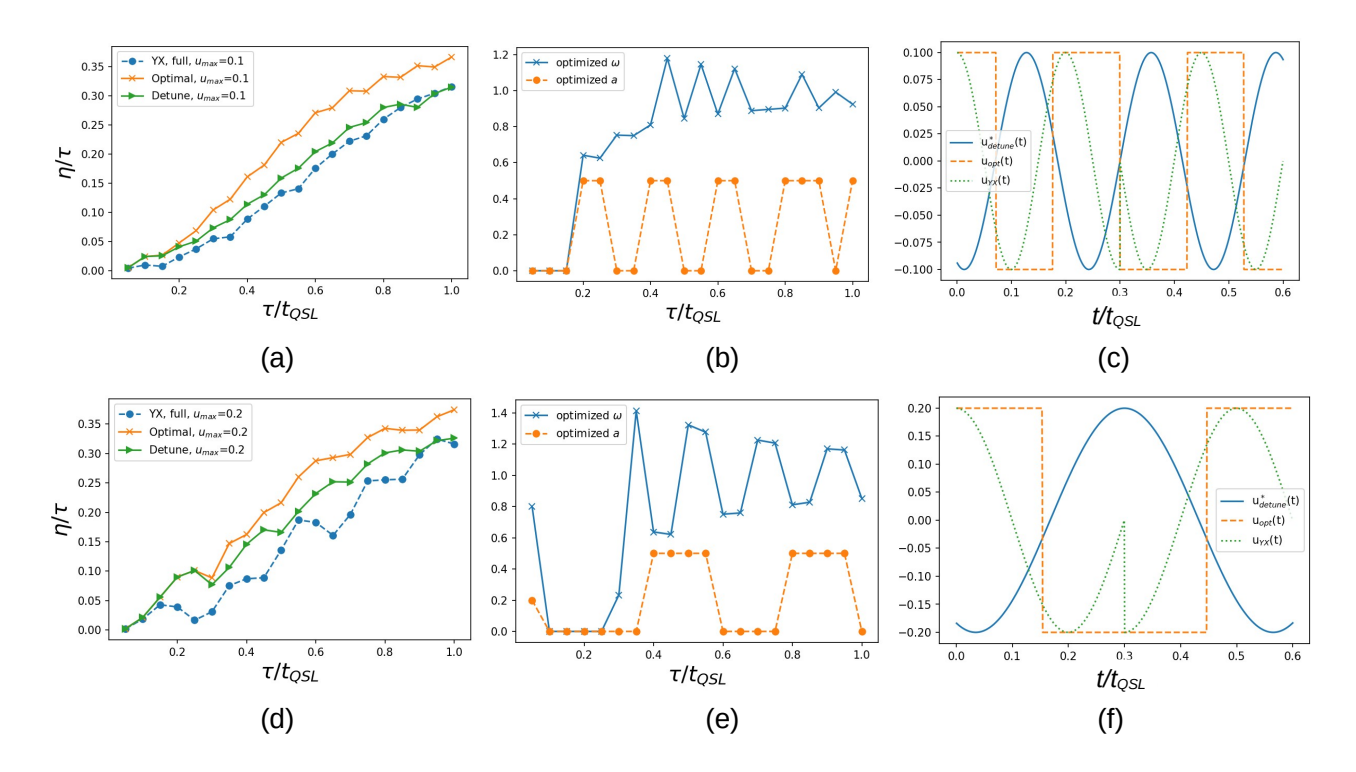


FIG. 4: η/τ obtained from the optimal, YX, and detune protocols as a function of τ ($\tau \in [0, t_{QSL}]$) for $u_{max} = 0.1$ (a) and 0.2 (d) using full calculation. The optimized detune parameters are given in (b) and (e). Notice that the a is either 0 or 0.5. The corresponding optimal, YX, and detune protocol for $\tau = 0.6 t_{QSL}$ are provided in (c) and (e). The main advantage of the detune protocol is its smoothness over the entire interrogation time.

D. Long interrogation time $\tau > T^*$

For completeness we consider the $\tau > T^*$ regime which is less relevant to high time resolution. In this regime the behavior is qualitatively similar to the celebrated Ramsey protocol [29]. In Fig. 5 we show the results for $u_{\text{max}} = 0.1$, 0.5 with the interrogation time $\tau = 1.2\,t_{\text{QSL}}$.

The optimal control can be divided into three stages. In the first stage the optimal control brings the quantum sensor to the equal-superposition of two natural eigenstates (equator on the Bloch sphere) using BB waveform in a very short time; this corresponds to the first $\frac{\pi}{2}$ pulse in Ramsey protocol and is demonstrated by the reduction of $\langle \sigma_z \rangle(t)$ from 1 to (near) 0 shown in Fig. 5(a), (c). The second stage is an S control which corresponds to the free evolution in the Ramsey protocol. One notes that in the optimal protocol the S control is not necessarily zero; particularly it can be significantly different from zero for large u_{max} as shown in Fig. 5(c). The final stage is again a BB control that maximizes the projection difference with and without $\delta\omega$. Overall for small $\frac{u_{\text{max}}}{\omega_0}$, the optimal protocol does behave like the Ramsey protocol; the main difference is that the initial and final $\frac{\pi}{2}$ pulses in the Ramsey sequence are replaced by the faster BB protocols [57].

We also compute the QFI [defined in Eq. (14)] that quantifies the sensing performance without specifying the measurement (i.e., with best possible measurement) and has an maximum value of t^2 for a two-level system [21, 25]. We find that QFI/ t^2 does not monotonically increase but slightly decreases in the final stage. For comparison, the protocols based on optimizing QFI are given in Fig. 5(b), (d) [26]. The QFI-optimized control brings the quantum sensor to the equator of the Bloch sphere and stops, as the state at the equator is indeed most sensitive to $\delta\omega \hat{\sigma}_z$; the resulting QFI/ t^2 keeps on increasing during the entire interrogation [dashed curves in Fig. 5(b), (d)]. However maximizing the QFI does not take the measurement into account, and in this case, it actually leads to zero sensitivity. This illustrates that QFI alone may not be sufficient to faithfully characterize the sensing performance under realistic conditions.

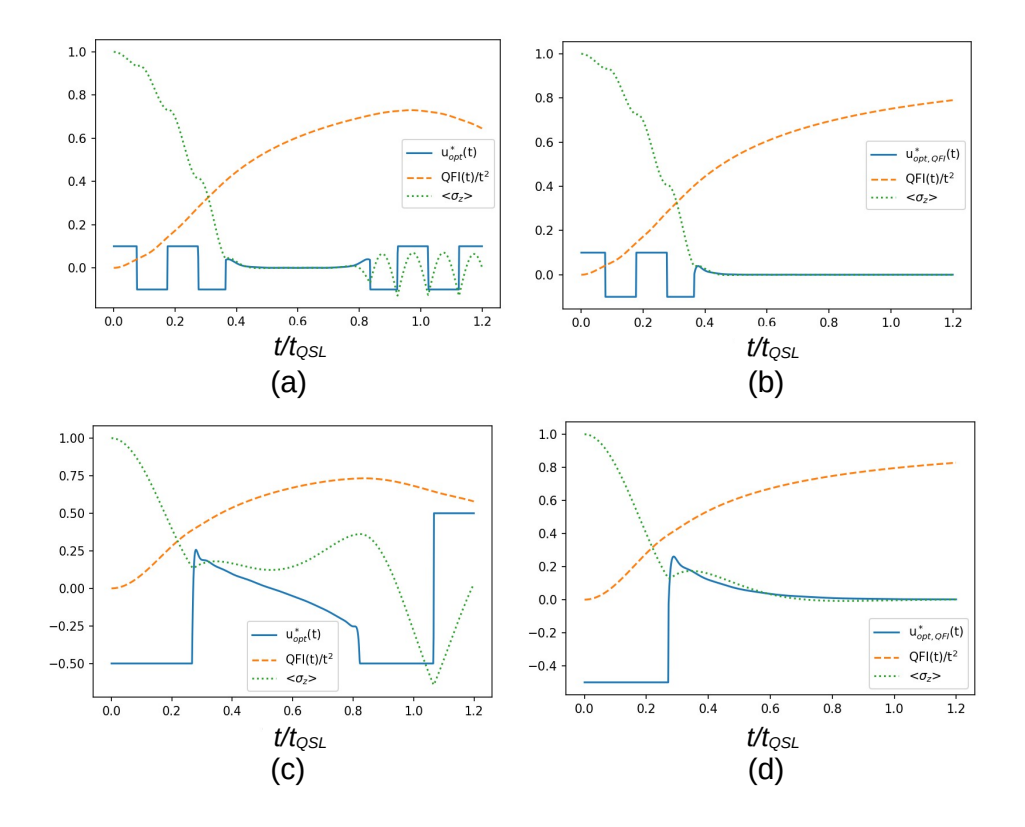


FIG. 5: Optimal controls that minimize C_{η^2} and $C_{\rm QFI}$ for $u_{\rm max}=0.1$ (a), (b) and $u_{\rm max}=0.5$ (c), (d). The corresponding QFI/ t^2 and $\langle \hat{\sigma}_z \rangle (t)$ are also present. The interrogation time is $\frac{\tau}{t_{\rm QSL}}=1.2$. The optimal control involves a singular arc in the middle, corresponding to the free evolution in the Ramsey protocol. According to $\langle \hat{\sigma}_z \rangle$, both η -optimal and QFI-optimal controls bring the quantum sensor to the equator of the Bloch sphere (i.e., $\langle \sigma_z \rangle = 0$) as soon as possible. To maximize QFI, the sensor stays on the equator. To maximize η , the optimal control induces some oscillation around the equator in the last stage of the interrogation.

IV. PRACTICAL CONSIDERATION

A. Smoothness and deviation from optimal performance

In this section, we address two practical issues related to short- τ time-resolution protocols. The short- τ optimal protocol is purely BB which contains discontinuities at switching times, and one can smooth the protocol by introducing a running cost that imposes smoothness. The degree of smoothness can be quantified by [57]

$$\mathcal{C}_{\text{smooth}}[u(t)] = \frac{1}{2} \int_0^{\tau} dt \, \dot{u}^2(t)
\Rightarrow \frac{\delta \mathcal{C}_{\text{smooth}}}{\delta u(t)} = -dt \, \ddot{u}.$$
(28)

The Neumann boundary condition $\dot{u}(0) = \dot{u}(\tau) = 0$ is used to determine \ddot{u} at two end points. To promote smoothness, the protocol is obtained by minimizing the total cost defined as

$$C_{\text{tot}} = C_{\eta^2} + W_{\text{smooth}}C_{\text{smooth}}, \tag{29}$$

where the weight W_{smooth} indicates the relative importance of smoothness. The resulting controls for $W_{\text{smooth}} = 0, 2, 10$ are shown in Fig. 6(a). Compared to the optimal BB protocol, imposing smoothness apparently smoothens the abrupt BB waveform, but the switching times (defined by u(t) = 0) are almost unchanged.

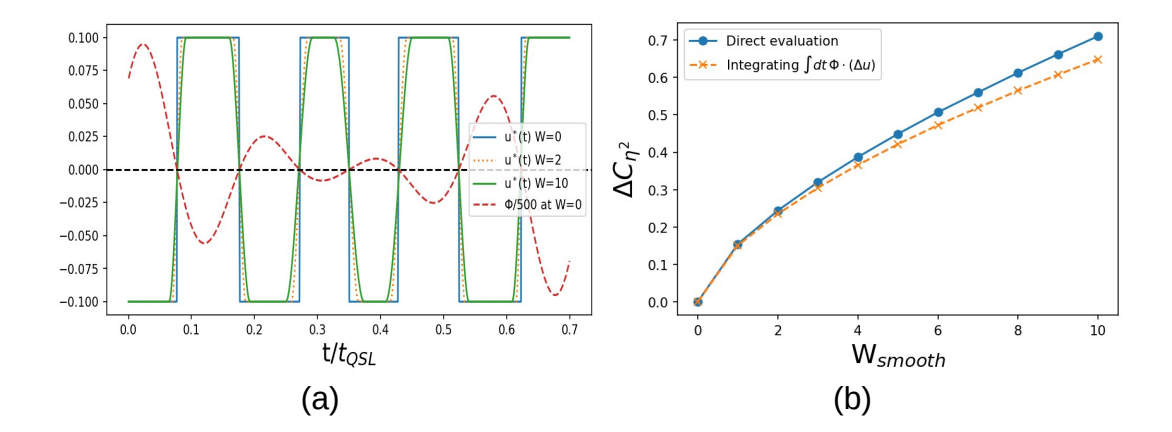


FIG. 6: Imposing smoothness and estimation of performance reduction. $u_{\text{max}} = 0.1$ is used in the calculation. (a) Optimal controls by minimizing Eq. (29) using W = 0, 2, 10. The switching function Φ is computed at $W_{\text{smooth}} = 0$. (b) The reduction of η^2 due to imposing smoothness, i.e., controls are obtained by minimizing \mathcal{C}_{tot} with W_{smooth} from 0 to 10. The difference between the direct evaluation and the first order approximation [last line of Eq. (30)] is within 10%.

The performance reduction resulting from smoothness can be estimated using Eq. (20); in this case,

$$\Delta C_{\eta^2} \equiv C_{\eta^2}[u_{\text{smooth}}(t)] - C_{\eta^2}[u^*(t)]$$

$$\approx \int dt \, \Phi(t)[u_{\text{smooth}}(t) - u^*(t)]$$
(30)

We have computed the reduction by directly evaluating C_{η^2} using two controls (first line of Eq. (30)) and by integrating over the product of switching function and the control difference [last line of Eq. (30)]. Their difference for $W_{\rm smooth} \in [0, 10]$ is shown in Fig. 6(b) and a very good agreement (< 10% difference) is seen. To obtain the reduction in sensitivity η , one uses $\Delta C_{\eta^2} = D\left[-\frac{\eta^2}{2}\right] = -|\eta|(\Delta \eta)$ to get $\Delta \eta = -\frac{\Delta C_{\eta^2}}{|\eta|}$.

B. Application to superconducting qubit

As stated at the end of Section II A, employing the time-resolution protocol requires a system capable of repeatedly generating the *identical*, yet unknown time-domain signal to be measured. Generating identical time-domain signals implies the ability of preparing the system of interest in exactly the *same* (but not necessarily known) initial state, which is the primary factor limiting its practical application. For example if the goal is to measure the magnetic domain wall propagation using the time-resolution protocol [30], one in principle needs to repeatedly prepare the system with a magnetic domain structure with nanometer-scale precision, which can be challenging. With the hardware constraints in mind, in the following we outline a potentially impactful application.

In the context of superconducting qubits, baseband flux pulses are widely used to implement quantum gates such as the physical Z gate, the iSWAP gate, and the controlled-phase (CPHASE) gate [62–73]. A long-standing challenge in these flux-based control schemes is pulse distortion – the deviation between the intended flux waveform and the actual waveform experienced by the qubit, arising from issues such as filtering effects and impedance mismatches in the control lines. To address this, we propose using the time-resolution protocol (preferably the detune variant) to characterize and compensate for these distortions. The procedure is illustrated in Fig. 7. In the example shown, the desired waveform is a known step pulse (blue, dashed curve), while the actual waveform experienced by the qubit is an unknown, distorted pulse (orange, solid curve). Good distortion calibration necessitates an accurate reconstruction of the distorted waveform. We apply the short- τ time-resolution protocol centered at a series of times t following the onset of the reference waveform, repeating each measurement many times to build sufficient statistics. Moreover since the commonly used dispersive readout of superconducting qubits belongs to the Quantum nondemolition (QND) measurement [74–76], i.e., the qubit remains in one of natural eigenstates following each short- τ

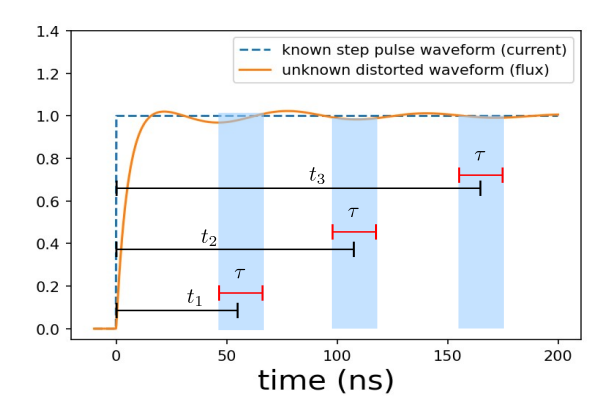


FIG. 7: Potential application in calibrating the Z pulse distortion in superconducting qubits. The distortion can have time constants ranging from tens of nanoseconds to microseconds [50, 51, 61]. The desired waveform is a step pulse (known) shown in blue and the actual waveform experienced by the qubit is a distorted pulse (unknown) shown in orange. Both are shown in arbitrary unit. To calibrate the distortion, we first need to reconstruct the distorted waveform. We apply the short- τ time-resolution protocol centered at a series of times t following the onset of the reference waveform, repeating each measurement many times to build sufficient statistics. For $u_{\text{max}} = 0.4$ GHz, the time resolution can be made smaller than $\tau \sim t_{\text{QSL}} = \frac{\pi}{u_{\text{max}}} = 8$ ns. In the plot $\tau \sim 20$ ns is used.

measurement, we can sequentially probe the same distorted waveform at different values of t, assuming the protocol does not significantly alter the profile of the distorted pulse. A complete calibration procedure using sequential measurements could substantially reduce the time required to collect sufficient data, thereby accelerating the overall calibration process.

To ensure clarity, the following three identifications are made for this application: the system of interest is the room-temperature-to-cryogenic electronics; the identical, unknown time-domain signal is the flux waveform on the cryogenic side generated by well controlled room-temperature electronics; the superconducting qubit, eventually controlled by the room-temperature electronics, functions as the sensor. Regardless of the sensor type (e.g., atoms, NV centers in diamond, ... etc), the time-resolution protocol appears suitable for calibrating known or distorted fields generated by the electronic devices, as the well-designed electronics can reliably produce identical signals. The justification for its use depends on the task at hand and the properties of the quantum sensor. For example the smallness of a quantum sensor enables detection at a precisely defined position, which is not easy or even possible for any other sensors. In this regard, using a qubit as a sensor to calibrate its own time-dependent control field is a natural fit, as it is inherently positioned in the optimal location.

V. CONCLUSION

We apply OCT to analyze the optimal performance of time resolution in quantum sensing. The performance of time resolution is quantified by the sensitivity with respect to the external field to be measured in a short interrogation time τ . For this task, an end-to-end description of the sensor state over the entire measurement process is essential as any operation contributes to the interrogation time. In particular, the initial state and the basis of projection measurement have to be in the natural eigenstates of the quantum sensor. One theoretical/numerical complication arising from time resolution when applying OCT is that the terminal cost involves the derivative of the quantum state, and we cope with this additional dependence by augmenting the dynamics. This procedure not only facilitates the numerics but keeps the control system time-invariant and control-affine so that the optimality conditions from OCT remains valid.

Similar to the reference YX protocol proposed in Ref. [28], the behavior of optimal protocols exhibits a critical interrogation time T^* : when $\tau < T^*$ the optimal protocol is purely bang-bang; when $\tau > T^*$ the optimal protocol involves a singular control the interrogation. The latter corresponds to the free evolution in the Ramsey protocol. Given the same amplitude constraint u_{max} , the optimal control achieves a higher sensitivity over the reference protocol.

The metrological gain is more substantial in the regime of short interrogation time, the regime relevant to high time resolution.

Despite the metrological gain in the short- τ regime, the bang-bang waveform of the optimal control contains several discontinuities, making it experimentally challenging to implement. The reference YX protocol is smoother but still carries one discontinuity at the midpoint of the interrogation. To address this issue, we propose a "detune protocol" that is smooth during the entire interrogation with performance comparable to (slightly better than) that of the reference YX protocol. An analytical approximation within RWA is derived, and physical intuition is developed based on Bloch sphere trajectories. We expect the detune protocol to be practically useful for the short- τ time-resolution protocol. In the long- τ regime, we evaluate QFI and construct the QFI-maximized protocols to illustrate the difference between theoretically optimal measurements (as indicated by QFI) and those that are practically realizable.

To meaningfully utilize the time-resolution protocol requires a setting in which the *identical*, yet unknown, time-domain signal can be generated repeatedly. As a potentially promising application, we propose using the time-resolution protocol to calibrate the waveform distortion between the intended flux waveform and the actual waveform experienced by a superconducting qubit. In this context, the superconducting qubit functions as a sensor. The advantages specific to this application, notably the QND-enabled sequential measurements, are discussed. We hope and expect that the proposed protocol will be useful for calibrating a qubit's control field.

Acknowledgment

We thank Junyoung An (MIT) for very insightful comments. C.L. thanks helpful discussions from Dries Sels (New York University and Flatiron Institute) and Yen-Hsiang Lin (National Tsing Hua University, Taiwan), and Chih-Chun Chien (University of California at Merced). Q. D. is grateful to William D. Oliver and Jeffery A. Grover for their support and helpful discussions.

Appendix A: Kernel function construction

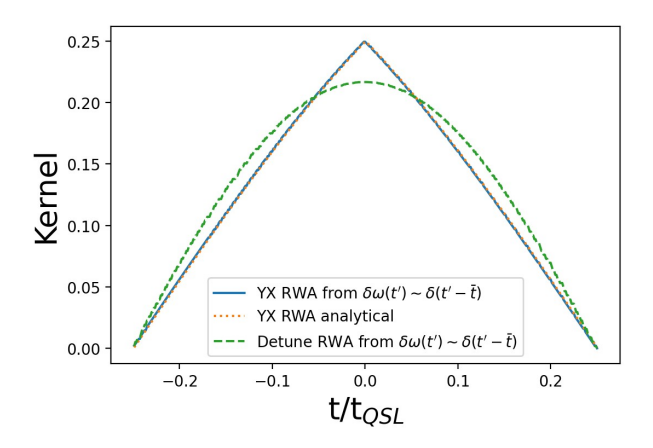


FIG. 8: RWA evaluated kernel functions [Eq. (8)] for YX and detune protocols. $u_{\rm max}=0.5$ and $\tau=0.5t_{\rm QSL}$ are used; the detune value is ~ 0.813 using Eq. (26). Numerical kernel function is constructed by applying a series of $\delta\omega(t')=\delta(t'-\bar{t})$ with 200 \bar{t} 's. For the YX protocol it matches well with the analytical expression [Eq. (A1)]. The kernel for the detune protocol is smoother. The integrated areas of both protocols are comparable because they have similar sensitivity values.

In this Appendix we provide a straightforward way to construct the kernel K in Eq. (8). Without loss of generality we take t=0 to simplify the notation. K(t') vanishes when $|t'| > \frac{\tau}{2}$ because during these periods the quantum sensor is in one of natural eigenstates (i.e., eigenstates of $\hat{\sigma}_z$) that does not respond to $\delta\omega$ $\hat{\sigma}_z$. When $\delta\omega(t') = \delta\omega$ is a constant over $|t'| < \frac{\tau}{2}$, the integrated area $\int dt' K(t') = \eta$.

The analytical expression for kernel function is not easy to derive if exists, but can be numerically constructed. The most straightforward way is to apply a sequence of $\delta\omega(t') = \delta(t'-\bar{t})$ for $\bar{t} \in [-\frac{\tau}{2}, +\frac{\tau}{2}]$, and at each \bar{t} the resulting $\delta p(0) = K(\bar{t})$. We test this method by constructing K of the YX protocol using RWA, and the profile agrees very well with the analytical expression

$$K(t') = \frac{\Theta(\frac{\tau}{2} - |t'|)}{2} \sin(\frac{u_{\text{max}}\tau}{2}) \cdot \sin(u_{\text{max}}(\frac{\tau}{2} - |t'|))$$
(A1)

given in Ref. [28]. Results for $\tau = 0.5\,t_{\rm QSL}$ for YX and detune protocols using RWA are given in Fig. 8. It is seen that the kernel of the detune protocol is smoother. The integrated areas of both protocols are comparable, indicating they have similar sensitivity values.

Appendix B: Second-order condition for singular control

Singular control $u^{\text{sing}}(t)$ given in Eq. (16) is determined by requiring $\Phi(t) = \dot{\Phi} = \ddot{\Phi} = 0$. In the following equations we only take the real part on the right-hand side:

$$\dot{\Phi} = (-i)^2 \langle \pi | \begin{bmatrix} \sigma_x & 0 \\ 0 & \sigma_x \end{bmatrix}, \begin{bmatrix} \frac{\omega_0}{2} \sigma_z & 0 \\ \frac{1}{2} \sigma_z & \frac{\omega_0}{2} \sigma_z \end{bmatrix}] | \psi \rangle = +2i \langle \pi | \begin{bmatrix} \frac{\omega_0}{2} \sigma_y & 0 \\ \frac{1}{2} \sigma_y & \frac{\omega_0}{2} \sigma_y \end{bmatrix} | \psi \rangle
\ddot{\Phi} = 4i \begin{pmatrix} \frac{\omega_0^2}{4} \Phi(t) + \frac{\omega_0}{2} \langle \pi | \begin{bmatrix} 0 & 0 \\ \sigma_x & 0 \end{bmatrix} | \psi \rangle - u^{\text{sing}}(t)(t) \langle \pi | \begin{bmatrix} \frac{\omega_0}{2} \sigma_z & 0 \\ \frac{1}{2} \sigma_z & \frac{\omega_0}{2} \sigma_z \end{bmatrix} | \psi \rangle \right) = 0.$$
(B1)

Using Re[-iA] = Im[A] leads to Eq. (16).

- C. L. Degen, F. Reinhard, and P. Cappellaro, Rev. Mod. Phys. 89, 035002 (2017), URL https://link.aps.org/doi/10. 1103/RevModPhys.89.035002.
- [2] M. Xiao, L.-A. Wu, and H. J. Kimble, Phys. Rev. Lett. 59, 278 (1987), URL https://link.aps.org/doi/10.1103/ PhysRevLett.59.278.
- [3] P. Grangier, R. E. Slusher, B. Yurke, and A. LaPorta, Phys. Rev. Lett. 59, 2153 (1987), URL https://link.aps.org/doi/10.1103/PhysRevLett.59.2153.
- [4] G. Breitenbach, S. Schiller, and J. Mlynek, Nature 387 (1997).
- [5] M. Tse, H. Yu, N. Kijbunchoo, A. Fernandez-Galiana, P. Dupej, L. Barsotti, C. D. Blair, D. D. Brown, S. E. Dwyer, A. Effler, et al., Phys. Rev. Lett. 123, 231107 (2019), URL https://link.aps.org/doi/10.1103/PhysRevLett.123. 231107.
- [6] F. Acernese, M. Agathos, L. Aiello, A. Allocca, A. Amato, S. Ansoldi, S. Antier, M. Arène, N. Arnaud, S. Ascenzi, et al. (Virgo Collaboration), Phys. Rev. Lett. 123, 231108 (2019), URL https://link.aps.org/doi/10.1103/PhysRevLett. 123.231108.
- [7] J. F. Barry, J. M. Schloss, E. Bauch, M. J. Turner, C. A. Hart, L. M. Pham, and R. L. Walsworth, Rev. Mod. Phys. 92, 015004 (2020), URL https://link.aps.org/doi/10.1103/RevModPhys.92.015004.
- [8] D. R. Glenn, D. B. Bucher, J. Lee, M. D. Lukin, H. Park, and R. L. Walsworth, Nature 555 (2018).
- [9] M. J. H. Ku, T. X. Zhou, Q. Li, Y. J. Shin, J. K. Shi, C. Burch, L. E. Anderson, A. T. Pierce, Y. Xie, A. Hamo, et al., Nature 583 (2020).
- [10] M. J. Turner, N. Langellier, R. Bainbridge, D. Walters, S. Meesala, T. M. Babinec, P. Kehayias, A. Yacoby, E. Hu, M. Lončar, et al., Phys. Rev. Appl. 14, 014097 (2020), URL https://link.aps.org/doi/10.1103/PhysRevApplied.14.014097.
- [11] M. Saffman, T. G. Walker, and K. Mølmer, Rev. Mod. Phys. 82, 2313 (2010), URL https://link.aps.org/doi/10.1103/ RevModPhys.82.2313.
- [12] J. A. Sedlacek, A. Schwettmann, H. Kübler, R. Löw, T. Pfau, and J. P. Shaffer, Nature Physics 18 (2012).
- [13] J. A. Sedlacek, A. Schwettmann, H. Kübler, and J. P. Shaffer, Phys. Rev. Lett. 111, 063001 (2013), URL https://link.aps.org/doi/10.1103/PhysRevLett.111.063001.
- [14] H. Q. Fan, S. Kumar, R. Daschner, H. Kübler, and J. P. Shaffer, Optics Letters 39 (2014).
- [15] D. H. Meyer, K. C. Cox, F. K. Fatemi, and P. D. Kunz, Applied Physics Letters 112, 211108 (2018), ISSN 0003-6951, https://pubs.aip.org/aip/apl/article-pdf/doi/10.1063/1.5028357/14511014/211108_1_online.pdf, URL https://doi.org/10.1063/1.5028357.

- [16] C. L. Holloway, M. T. Simons, A. H. Haddab, C. J. Williams, and M. W. Holloway, AIP Advances 9, 065110 (2019), ISSN 2158-3226, URL https://doi.org/10.1063/1.5099036.
- [17] L. A. Downes, A. R. MacKellar, D. J. Whiting, C. Bourgenot, C. S. Adams, and K. J. Weatherill, Phys. Rev. X 10, 011027 (2020), URL https://link.aps.org/doi/10.1103/PhysRevX.10.011027.
- [18] M. Cloutman, M. Chilcott, A. Elliott, J. S. Otto, A. B. Deb, and N. Kjærgaard, Phys. Rev. Appl. 21, 044025 (2024), URL https://link.aps.org/doi/10.1103/PhysRevApplied.21.044025.
- [19] C. W. Helstrom, Quantum Detection and Estimation Theory, Mathematics in Science and Engineering 123 (Elsevier, Academic Press, 1976).
- [20] A. S. Holevo, Probabilistic and Statistical Aspects of Quantum Theory (Edizioni della Normale, 2011), 1st ed.
- [21] V. Giovannetti, S. Lloyd, and L. Maccone, Phys. Rev. Lett. 96, 010401 (2006), URL https://link.aps.org/doi/10. 1103/PhysRevLett.96.010401.
- [22] V. Giovannetti, S. Lloyd, and L. Maccone, Nature Photonics 5, 222 (2011).
- [23] J. Liu and H. Yuan, Phys. Rev. A 96, 012117 (2017), URL https://link.aps.org/doi/10.1103/PhysRevA.96.012117.
- [24] J. Liu and H. Yuan, Phys. Rev. A 96, 042114 (2017), URL https://link.aps.org/doi/10.1103/PhysRevA.96.042114.
- [25] S. A. Haine and J. J. Hope, Phys. Rev. Lett. 124, 060402 (2020), URL https://link.aps.org/doi/10.1103/PhysRevLett. 124.060402.
- [26] C. Lin, Y. Ma, and D. Sels, Phys. Rev. A 103, 052607 (2021), URL https://link.aps.org/doi/10.1103/PhysRevA.103. 052607.
- [27] C. Lin, Y. Ma, and D. Sels, Phys. Rev. A 105, 042621 (2022), URL https://link.aps.org/doi/10.1103/PhysRevA.105. 042621.
- [28] K. Herb and C. L. Degen, Phys. Rev. Lett. 133, 210802 (2024), URL https://link.aps.org/doi/10.1103/PhysRevLett. 133.210802.
- [29] N. F. Ramsey, Phys. Rev. 78, 695 (1950), URL https://link.aps.org/doi/10.1103/PhysRev.78.695.
- [30] K. Herb, L. A. Völker, J. M. Abendroth, N. Meinhardt, L. van Schie, P. Gambardella, and C. L. Degen, Nature Communications 16 (2025), ISSN 2041-1723, URL http://dx.doi.org/10.1038/s41467-025-55956-1.
- [31] D. G. Luenberger, Introduction to dynamic systems: theory, models, and applications (Wiley, New York, 1979).
- [32] D. Liberzon, Calculus of Variations and Optimal Control Theory: A Concise Introduction (Princeton University Press, 2012).
- [33] U. L. Heinz Schattler, Geometric Optimal Control: Theory, Methods and Examples, Interdisciplinary Applied Mathematics 38 (Springer-Verlag New York, 2012), 1st ed., ISBN 978-1-4614-3833-5,978-1-4614-3834-2.
- [34] L. Pontryagin, Mathematical Theory of Optimal Processes (CRC Press, Boca Raton, FL, 1987).
- [35] P. Rembold, N. Oshnik, M. M. Müller, S. Montangero, T. Calarco, and E. Neu, AVS Quantum Science 2, 024701 (2020), URL https://doi.org/10.1116/5.0006785.
- [36] U. Boscain, M. Sigalotti, and D. Sugny, PRX Quantum 2, 030203 (2021), URL https://link.aps.org/doi/10.1103/ PRXQuantum.2.030203.
- [37] A. B. Magann, C. Arenz, M. D. Grace, T.-S. Ho, R. L. Kosut, J. R. McClean, H. A. Rabitz, and M. Sarovar, PRX Quantum 2, 010101 (2021), URL https://link.aps.org/doi/10.1103/PRXQuantum.2.010101.
- [38] Q. Ansel, E. Dionis, F. Arrouas, B. Peaudecerf, S. Guérin, D. Guéry-Odelin, and D. Sugny, *Introduction to theoretical and experimental aspects of quantum optimal control* (2024), arXiv: 2403.00532.
- [39] C. P. Koch, J. P. Palao, R. Kosloff, and F. m. c. Masnou-Seeuws, Phys. Rev. A 70, 013402 (2004), URL https://link.aps.org/doi/10.1103/PhysRevA.70.013402.
- [40] M. Lapert, E. Assémat, S. J. Glaser, and D. Sugny, Phys. Rev. A 90, 023411 (2014), URL https://link.aps.org/doi/10.1103/PhysRevA.90.023411.
- [41] K. Kobzar, S. Ehni, T. E. Skinner, S. J. Glaser, and B. Luy, Journal of Magnetic Resonance 225, 142 (2012), ISSN 1090-7807, URL https://www.sciencedirect.com/science/article/pii/S1090780712003126.
- [42] G. Dridi, M. Mejatty, S. J. Glaser, and D. Sugny, Phys. Rev. A 101, 012321 (2020), URL https://link.aps.org/doi/ 10.1103/PhysRevA.101.012321.
- [43] D. Stefanatos, J. Ruths, and J.-S. Li, Phys. Rev. A 82, 063422 (2010), URL https://link.aps.org/doi/10.1103/ PhysRevA.82.063422.
- [44] D. Stefanatos, H. Schaettler, and J.-S. Li, SIAM Journal on Control and Optimization 49, 2440 (2011), URL https://doi.org/10.1137/100818431.
- [45] A. Rahmani, T. Kitagawa, E. Demler, and C. Chamon, Phys. Rev. A 87, 043607 (2013), URL https://link.aps.org/doi/10.1103/PhysRevA.87.043607.
- [46] J. Cai, G. G. Guerreschi, and H. J. Briegel, Phys. Rev. Lett. 104, 220502 (2010), URL https://link.aps.org/doi/10. 1103/PhysRevLett.104.220502.
- [47] L. D. Smith, F. T. Chowdhury, I. Peasgood, N. Dawkins, and D. R. Kattnig, The Journal of Physical Chemistry Letters 13, 10500 (2022), pMID: 36332112, https://doi.org/10.1021/acs.jpclett.2c02840, URL https://doi.org/10.1021/acs.jpclett.2c02840.

- [48] F. T. Chowdhury, M. C. Denton, D. C. Bonser, and D. R. Kattnig, PRX Quantum 5, 020303 (2024), URL https://link.aps.org/doi/10.1103/PRXQuantum.5.020303.
- [49] L. D. Smith, F. T. Chowdhury, J. Glatthard, and D. R. Kattnig, Interradical motion can push magnetosensing precision towards quantum limits (2025), 2506.21389, URL https://arxiv.org/abs/2506.21389.
- [50] M. A. Rol, L. Ciorciaro, F. K. Malinowski, B. M. Tarasinski, R. E. Sagastizabal, C. C. Bultink, Y. Salathe, N. Haandbaek, J. Sedivy, and L. DiCarlo, Applied Physics Letters 116, 054001 (2020), ISSN 0003-6951, https://pubs.aip.org/aip/apl/article-pdf/doi/10.1063/1.5133894/14531145/054001_1_online.pdf, URL https://doi.org/ 10.1063/1.5133894.
- [51] C. Hellings, N. Lacroix, A. Remm, R. Boell, J. Herrmann, S. Lazăr, S. Krinner, F. Swiadek, C. K. Andersen, C. Eichler, et al., Calibrating magnetic flux control in superconducting circuits by compensating distortions on time scales from nanoseconds up to tens of microseconds (2025), 2503.04610, URL https://arxiv.org/abs/2503.04610.
- [52] T.-M. Li, J.-C. Zhang, B.-J. Chen, K. Huang, H.-T. Liu, Y.-X. Xiao, C.-L. Deng, G.-H. Liang, C.-T. Chen, Y. Liu, et al., Physical Review Applied 23 (2025), ISSN 2331-7019, URL http://dx.doi.org/10.1103/PhysRevApplied.23.024059.
- [53] The quantum speed limit in this context refers to the minimum time required to guide the qubit from $|0\rangle$ or $|1\rangle$ (i.e., one of poles on the Bloch sphere) to the state of equal superposition of $|0\rangle$ and $|1\rangle$ (i.e., the equator on the Bloch sphere) given $u(t) = u_{\text{max}} \cos(\omega_0 t)$ using RWA.
- [54] L. Mandelstam and I. Tamm, J. Phys. (USSR) 9, 249 (1945).
- [55] N. Margolus and L. B. Levitin, Physica D 120, 188 (1998).
- [56] S. Deffner and S. Campbell, Journal of Physics A: Mathematical and Theoretical 50, 453001 (2017), URL https://dx.doi.org/10.1088/1751-8121/aa86c6.
- [57] C. Lin, Q. Ding, P. T. Boufounos, Y. Ma, Y. Wang, D. Sels, and C.-C. Chien, Phys. Rev. A 111, 042602 (2025), URL https://link.aps.org/doi/10.1103/PhysRevA.111.042602.
- [58] C. Lin, D. Sels, and Y. Wang, Phys. Rev. A 101, 022320 (2020), URL https://link.aps.org/doi/10.1103/PhysRevA. 101.022320.
- [59] Rigorously these two optimality conditions hold only when the control dynamics is control-affine [linear in u(t)] and time-invariant [the time dependence is solely from u(t)]. The augmented dynamics of Eq. (12c) meets these two conditions.
- [60] N. Khaneja, T. Reiss, C. Kehlet, T. Schulte-Herbrüggen, and S. J. Glaser, Journal of Magnetic Resonance 172, 296 (2005), ISSN 1090-7807, URL http://www.sciencedirect.com/science/article/pii/S1090780704003696.
- [61] T.-M. Li, J.-C. Zhang, B.-J. Chen, K. Huang, H.-T. Liu, Y.-X. Xiao, C.-L. Deng, G.-H. Liang, C.-T. Chen, Y. Liu, et al., Phys. Rev. Appl. 23, 024059 (2025), URL https://link.aps.org/doi/10.1103/PhysRevApplied.23.024059.
- [62] M. Kjaergaard, M. E. Schwartz, A. Greene, G. O. Samach, A. Bengtsson, M. O'Keeffe, C. M. McNally, J. Braumüller, D. K. Kim, P. Krantz, et al., Phys. Rev. X 12, 011005 (2022), URL https://link.aps.org/doi/10.1103/PhysRevX.12.011005.
- [63] V. Negîrneac, H. Ali, N. Muthusubramanian, F. Battistel, R. Sagastizabal, M. S. Moreira, J. F. Marques, W. J. Vlothuizen, M. Beekman, C. Zachariadis, et al., Phys. Rev. Lett. 126, 220502 (2021), URL https://link.aps.org/doi/10.1103/PhysRevLett.126.220502.
- [64] X. Y. Jin, S. Gustavsson, J. Bylander, F. Yan, F. Yoshihara, Y. Nakamura, T. P. Orlando, and W. D. Oliver, Phys. Rev. Appl. 3, 034004 (2015), URL https://link.aps.org/doi/10.1103/PhysRevApplied.3.034004.
- [65] R. Barends, J. Kelly, A. Megrant, A. Veitia, D. Sank, E. Jeffrey, T. C. White, J. Mutus, A. G. Fowler, B. Campbell, et al., Nature 508, 500 (2014), ISSN 1476-4687, URL https://www.nature.com/articles/nature13171.
- [66] P. Krantz, M. Kjaergaard, F. Yan, T. P. Orlando, S. Gustavsson, and W. D. Oliver, Applied Physics Reviews 6 (2019), ISSN 1931-9401, URL http://dx.doi.org/10.1063/1.5089550.
- [67] Q. Ding, A. V. Oppenheim, P. T. Boufounos, S. Gustavsson, J. A. Grover, T. A. Baran, and W. D. Oliver, Phys. Rev. Appl. 23, 064013 (2025), URL https://link.aps.org/doi/10.1103/yskp-mfcr.
- [68] Y. Chen, K. N. Nesterov, V. E. Manucharyan, and M. G. Vavilov, Phys. Rev. Appl. 18, 034027 (2022), URL https://link.aps.org/doi/10.1103/PhysRevApplied.18.034027.
- [69] M. C. Collodo, J. Herrmann, N. Lacroix, C. K. Andersen, A. Remm, S. Lazar, J.-C. Besse, T. Walter, A. Wallraff, and C. Eichler, Phys. Rev. Lett. 125, 240502 (2020), URL https://link.aps.org/doi/10.1103/PhysRevLett.125.240502.
- [70] J. Chu and F. Yan, Physical Review Applied 16, 054020 (2021), URL https://link.aps.org/doi/10.1103/PhysRevApplied.16.054020.
- [71] J. Kelly, R. Barends, B. Campbell, Y. Chen, Z. Chen, B. Chiaro, A. Dunsworth, A. G. Fowler, I.-C. Hoi, E. Jeffrey, et al., Phys. Rev. Lett. 112, 240504 (2014), URL https://link.aps.org/doi/10.1103/PhysRevLett.112.240504.
- [72] Y. Sung, L. Ding, J. Braumüller, A. Vepsäläinen, B. Kannan, M. Kjaergaard, A. Greene, G. O. Samach, C. McNally, D. Kim, et al., Phys. Rev. X 11, 021058 (2021), URL https://link.aps.org/doi/10.1103/PhysRevX.11.021058.
- [73] P. Zhao, R. Wang, M.-J. Hu, T. Ma, P. Xu, Y. Jin, and H. Yu, Phys. Rev. Appl. 19, 054050 (2023), URL https://link.aps.org/doi/10.1103/PhysRevApplied.19.054050.
- [74] A. Blais, R.-S. Huang, A. Wallraff, S. M. Girvin, and R. J. Schoelkopf, Phys. Rev. A 69, 062320 (2004), URL https://link.aps.org/doi/10.1103/PhysRevA.69.062320.
- [75] A. Blais, A. L. Grimsmo, S. M. Girvin, and A. Wallraff, Rev. Mod. Phys. 93, 025005 (2021), URL https://link.aps.

org/doi/10.1103/RevModPhys.93.025005.

[76] A. Lupascu, S. Saito, T. Picot, P. de Groot, C. J. P. M. Harmans, and J. E. Mooij, Nature Physics 3 (2007).